Biomedical Optics EXPRESS

Designed Er^{3+}-singly doped $NaYF_4$ with double excitation bands for simultaneous deep macroscopic and microscopic upconverting bioimaging

Xuanyuan Wen,[1] Baoju Wang,[1] Ruitao Wu,[1] Nana Li,[1] Sailing He,[1,2] and Qiuqiang Zhan[1,*]

[1]*Centre for Optical and Electromagnetic Research, South China Academy of Advanced Optoelectronics, South China Normal University, 510006 Guangzhou, China*

[2]*Department of Electromagnetic Engineering, Royal Institute of Technology, 10044 Stockholm, Sweden*

[*]*zhanqiuqiang@m.scnu.edu.cn*

Abstract: Simultaneous deep macroscopic imaging and microscopic imaging is in urgent demand, but is challenging to achieve experimentally due to the lack of proper fluorescent probes. Herein, we have designed and successfully synthesized simplex Er^{3+}-doped upconversion nanoparticles (UCNPs) with double excitation bands for simultaneous deep macroscopic and microscopic imaging. The material structure and the excitation wavelength of Er^{3+}-singly doped UCNPs were further optimized to enhance the upconversion emission efficiency. After optimization, we found that $NaYF_4$:30%Er^{3+}@$NaYF_4$:2%Er^{3+} could simultaneously achieve efficient two-photon excitation (2PE) macroscopic tissue imaging and three-photon excitation (3PE) deep microscopic when excited by 808 nm continuous wave (CW) and 1480 nm CW lasers, respectively. *In vitro* cell imaging and *in vivo* imaging have also been implemented to demonstrate the feasibility and potential of the proposed simplex Er^{3+}-doped UCNPs as bioprobe.

©2016 Optical Society of America

OCIS codes: (160.5690) Rare-earth-doped materials; (170.2520) Fluorescence microscopy; (190.4180) Multiphoton processes; (180.0180) Microscopy.

References and links

1. N. G. Horton, K. Wang, D. Kobat, C. G. Clark, F. W. Wise, C. B. Schaffer, and C. Xu, "*In vivo* three-photon microscopy of subcortical structures within an intact mouse brain," Nat. Photonics **7**(3), 205–209 (2013).
2. Q. Zhan, J. Qian, H. Liang, G. Somesfalean, D. Wang, S. He, Z. Zhang, and S. Andersson-Engels, "Using 915 nm laser excited Tm^3+/Er^3+/Ho^3+- doped $NaYbF_4$ upconversion nanoparticles for in vitro and deeper in vivo bioimaging without overheating irradiation," ACS Nano **5**(5), 3744–3757 (2011).
3. S. V. Eliseeva and J.-C. G. Bünzli, "Lanthanide luminescence for functional materials and bio-sciences," Chem. Soc. Rev. **39**(1), 189–227 (2010).
4. H. Kobayashi, M. Ogawa, R. Alford, P. L. Choyke, and Y. Urano, "New strategies for fluorescent probe design in medical diagnostic imaging," Chem. Rev. **110**(5), 2620–2640 (2010).
5. L. Cheng, K. Yang, Y. Li, J. Chen, C. Wang, M. Shao, S. T. Lee, and Z. Liu, "Facile preparation of multifunctional upconversion nanoprobes for multimodal imaging and dual-targeted photothermal therapy," Angew. Chem. Int. Ed. Engl. **50**(32), 7385–7390 (2011).
6. J. Xie, G. Liu, H. S. Eden, H. Ai, and X. Chen, "Surface-engineered magnetic nanoparticle platforms for cancer imaging and therapy," Acc. Chem. Res. **44**(10), 883–892 (2011).
7. H. S. Mader, P. Kele, S. M. Saleh, and O. S. Wolfbeis, "Upconverting luminescent nanoparticles for use in bioconjugation and bioimaging," Curr. Opin. Chem. Biol. **14**(5), 582–596 (2010).
8. B. Wang, Q. Zhan, Y. Zhao, R. Wu, J. Liu, and S. He, "Visible-to-visible four-photon ultrahigh resolution microscopic imaging with 730-nm diode laser excited nanocrystals," Opt. Express **24**(2), A302–A311 (2016).
9. N. Li, X. Wen, J. Liu, B. Wang, Q. Zhan, and S. He, "Yb^{3+}-enhanced UCNP@ SiO_2 nanocomposites for consecutive imaging, photothermal-controlled drug delivery and cancer therapy," Opt. Mater. Express **6**(4), 1161–1171 (2016).

#264009 Received 29 Apr 2016; revised 9 May 2016; accepted 9 May 2016; published 13 May 2016

10. Q. Q. Zhan, X. Zhang, Y. X. Zhao, J. Liu, and S. L. He, "Tens of thousands-fold upconversion luminescence enhancement induced by a single gold nanorod," Laser Photonics Rev. **9**(5), 479–487 (2015).
11. M. Haase and H. Schäfer, "Upconverting nanoparticles," Angew. Chem. Int. Ed. Engl. **50**(26), 5808–5829 (2011).
12. F. Auzel, "Upconversion and anti-Stokes processes with f and d ions in solids," Chem. Rev. **104**(1), 139–174 (2004).
13. F. Wang and X. Liu, "Recent advances in the chemistry of lanthanide-doped upconversion nanocrystals," Chem. Soc. Rev. **38**(4), 976–989 (2009).
14. X. Li, F. Zhang, and D. Zhao, "Lab on upconversion nanoparticles: optical properties and applications engineering via designed nanostructure," Chem. Soc. Rev. **44**(6), 1346–1378 (2015).
15. X. Wu, Y. Zhang, K. Takle, O. Bilsel, Z. Li, H. Lee, Z. Zhang, D. Li, W. Fan, C. Duan, E. M. Chan, C. Lois, Y. Xiang, and G. Han, "Dye-Sensitized Core/Active Shell Upconversion Nanoparticles for Optogenetics and Bioimaging Applications," ACS Nano **10**(1), 1060–1066 (2016).
16. Y. Zhang, L. Huang, Z. Li, G. Ma, Y. Zhou, and G. Han, "Illuminating Cell Signaling with Near-Infrared Light-Responsive Nanomaterials," ACS Nano **10**(4), 3881–3885 (2016).
17. L. He, Y. Zhang, G. Ma, P. Tan, Z. Li, S. Zang, X. Wu, J. Jing, S. Fang, L. Zhou, Y. Wang, Y. Huang, P. G. Hogan, G. Han, and Y. Zhou, "Near-infrared photoactivatable control of Ca^{2+} signaling and optogenetic immunomodulation," eLife **4**, 10024 (2015).
18. X. Wu, H. Lee, O. Bilsel, Y. Zhang, Z. Li, T. Chen, Y. Liu, C. Duan, J. Shen, A. Punjabi, and G. Han, "Tailoring dye-sensitized upconversion nanoparticle excitation bands towards excitation wavelength selective imaging," Nanoscale **7**(44), 18424–18428 (2015).
19. G. Chen, T. Y. Ohulchanskyy, A. Kachynski, H. Agren, and P. N. Prasad, "Intense visible and near-infrared upconversion photoluminescence in colloidal $LiYF_4:Er^{3+}$ nanocrystals under excitation at 1490 nm," ACS Nano **5**(6), 4981–4986 (2011).
20. J. Liu, R. Wu, N. Li, X. Zhang, Q. Zhan, and S. He, "Deep, high contrast microscopic cell imaging using three-photon luminescence of β-($NaYF_4:Er^{3+}/NaYF_4$) nanoprobe excited by 1480-nm CW laser of only 1.5-mW," Biomed. Opt. Express **6**(5), 1857–1866 (2015).
21. X. Shang, P. Chen, T. Jia, D. Feng, S. Zhang, Z. Sun, and J. Qiu, "Upconversion luminescence mechanisms of Er^{3+} ions under excitation of an 800 nm laser," Phys. Chem. Chem. Phys. **17**(17), 11481–11489 (2015).
22. D. Wang, B. Xue, X. Kong, L. Tu, X. Liu, Y. Zhang, Y. Chang, Y. Luo, H. Zhao, and H. Zhang, "808 nm driven Nd^{3+}-sensitized upconversion nanostructures for photodynamic therapy and simultaneous fluorescence imaging," Nanoscale **7**(1), 190–197 (2015).
23. Z. Wang, P. Zhang, Q. Yuan, X. Xu, P. Lei, X. Liu, Y. Su, L. Dong, J. Feng, and H. Zhang, "Nd^{3+}-sensitized $NaLuF_4$ luminescent nanoparticles for multimodal imaging and temperature sensing under 808 nm excitation," Nanoscale **7**(42), 17861–17870 (2015).
24. Y. Zhong, G. Tian, Z. Gu, Y. Yang, L. Gu, Y. Zhao, Y. Ma, and J. Yao, "Elimination of photon quenching by a transition layer to fabricate a quenching-shield sandwich structure for 800 nm excited upconversion luminescence of Nd^{3+}-sensitized nanoparticles," Adv. Mater. **26**(18), 2831–2837 (2014).
25. Q. Zhan, B. Wang, X. Wen, and S. He, "Controlling the excitation of upconverting luminescence for biomedical theranostics: neodymium sensitizing," Opt. Mater. Express **6**(4), 1011–1023 (2016).
26. F. Wang, R. Deng, and X. Liu, "Preparation of core-shell $NaGdF_4$ nanoparticles doped with luminescent lanthanide ions to be used as upconversion-based probes," Nat. Protoc. **9**(7), 1634–1644 (2014).
27. N. Bogdan, F. Vetrone, G. A. Ozin, and J. A. Capobianco, "Synthesis of ligand-free colloidally stable water dispersible brightly luminescent lanthanide-doped upconverting nanoparticles," Nano Lett. **11**(2), 835–840 (2011).
28. G. Chen, T. Y. Ohulchanskyy, S. Liu, W. C. Law, F. Wu, M. T. Swihart, H. Agren, and P. N. Prasad, "Core/shell $NaGdF_4:Nd^{3+}/NaGdF_4$ nanocrystals with efficient near-infrared to near-infrared downconversion photoluminescence for bioimaging applications," ACS Nano **6**(4), 2969–2977 (2012).
29. G. M. Spirou, A. A. Oraevsky, I. A. Vitkin, and W. M. Whelan, "Optical and acoustic properties at 1064 nm of polyvinyl chloride-plastisol for use as a tissue phantom in biomedical optoacoustics," Phys. Med. Biol. **50**(14), N141–N153 (2005).
30. B. W. Pogue and M. S. Patterson, "Review of tissue simulating phantoms for optical spectroscopy, imaging and dosimetry," J. Biomed. Opt. **11**(4), 041102 (2006).
31. V. V. Tuchin, and Society of Photo-optical Instrumentation Engineers, *Tissue optics: light scattering methods and instruments for medical diagnosis* (SPIE/International Society for Optical Engineering, Bellingham, Wash., 2007).
32. J. Shen, G. Y. Chen, A. M. Vu, W. Fan, O. S. Bilsel, C. C. Chang, and G. Han, "Engineering the Upconversion Nanoparticle Excitation Wavelength: Cascade Sensitization of Tri-doped Upconversion Colloidal Nanoparticles at 800 nm," Adv. Opt. Mater. **1**(9), 644–650 (2013).
33. Y. Zhao, Q. Zhan, J. Liu, and S. He, "Optically investigating Nd^{3+}-Yb^{3+} cascade sensitized upconversion nanoparticles for high resolution, rapid scanning, deep and damage-free bio-imaging," Biomed. Opt. Express **6**(3), 838–848 (2015).
34. M. Pollnau, D. R. Gamelin, S. R. Luthi, H. U. Gudel, and M. P. Hehlen, "Power dependence of upconversion luminescence in lanthanide and transition-metal-ion systems," Phys. Rev. B **61**(5), 3337–3346 (2000).
35. G. Chen, H. Qiu, P. N. Prasad, and X. Chen, "Upconversion nanoparticles: design, nanochemistry, and applications in theranostics," Chem. Rev. **114**(10), 5161–5214 (2014).

#264009 Received 29 Apr 2016; revised 9 May 2016; accepted 9 May 2016; published 13 May 2016
(C) 2016 OSA

1. Introduction

Optical imaging plays a major role in laboratorial biomedical research as well as clinical diagnostics. Macroscopic imaging (*e.g.*, diffusion fluorescence imaging) and microscopic imaging are two commonly used optical bioimaging modalities, providing non-invasive or minimally invasive imaging of biological sample. However, optical image acquisition through significant depths of biological tissue presents a major scientific challenge since tissue is extremely heterogeneous, and the strong scattering of various tissue components has historically restricted high-resolution microscopic imaging to thin slices or to superficial layers. To achieve the maximal imaging depth in high resolution microscopic imaging, combining near infrared long wavelength (1200-1700 nm) excited bioimaging probe with multi-photon fluorescence microscopy (*e.g.*, three-photon microscopy) is an alternative solution. Since the long wavelength light would greatly suppress the scattering, and three-photon excitation (3PE) can dramatically reduce the background from the regions far from the focal plane, improving the signal-to-background ratio (SBR) by several orders of magnitude when compared to two-photon excitation (2PE) microscopic imaging [1]. By contrast, for *in vivo* macroscopic imaging, absorption is a major concern for imaging depth since the large attenuation of excitation light would limit the imaging depth and also induce overheating effects. The near-infrared (NIR) region at around 700-920 nm is an ideal excitation wavelength for *in vivo* macroscopic imaging, reaching a minimum absorbance for all bio-molecules [2].

Simultaneous deep macroscopic imaging and microscopic imaging is in urgent demand. For example, one could find the tumor location after macroscopic *in vivo* imaging using fluorescent biomarker. Afterwards, microscopic imaging of the tumor tissue section is necessary for further pathological diagnostics. The lack of the biomarkers capable of achieving these two imaging processes simultaneously leads to a two-step labeling process, which makes the whole imaging procedure complicated and inefficient. Furthermore, for certain *in vivo* imaging applications, the *in vivo* deep microscopic imaging need to be immediately carried out, following the diffusion optical imaging that search for the range of interests. However, the contradictory requirements on two different excitation wavelengths make these two optical imaging modalities challenging to be simultaneously achieved. Therefore, the development of a single optical probe to be efficiently excited by both the long wavelength (1200-1700 nm) laser and the short one (700-920 nm) is of high significance.

In the past decade, upconversion nanoparticles (UCNPs) have been emerging as an important class of nanomaterials owing to their wide applications in solid-state lasers, optical biosensing, and optical bioimaging [3–10]. All these applications benefit from the distinguished merits of UCNPs, including tunable excitation, narrow band emissions, large anti-Stokes shifts, long lifetimes, superior stability, low toxicity, weak fluorescence background [11–14]. In addition, the absorption range of UCNPs can be broadened and the upconversion efficiency can be boosted using NIR dye-sensitized UCNPs [15–18]. Superior to other kinds of fluophores, UCNPs has the unique property of multiple excitation bands and holds the potential to achieve simultaneous deep microscopic and macroscopic upconversion imaging. Er^{3+}-doped UCNPs have strong three-photon emission under the excitation of 1450-1580 nm band light due to the $^4I_{15/2}\rightarrow{}^4I_{13/2}$ transition which can be exploited to implement three-photon microscopic imaging (3PM) [19]. Recently, Zhan *et al.* achieved deep microscopic imaging by the use of the intense emission of Er^{3+}-doped $NaYF_4$ UCNPs [20]. Although it has been found that Er^{3+} can be excited with an 800 nm laser [21], the excitation efficiency was too low to perform tissue imaging compared to the commonly used 800 nm-excited Nd^{3+}-doped UCNPs. However, the Nd^{3+}-doped UCNPs cannot be efficiently excited by long wavelength (> 1000 nm) for deep microscopic imaging. Furthermore, multilayer core-shell structures are needed to minimize the quenching effect between the

#264009 Received 29 Apr 2016; revised 9 May 2016; accepted 9 May 2016; published 13 May 2016
(C) 2016 OSA

activators and Nd^{3+} ions, which require sophisticated design and synthesis [22–25]. To the best of our knowledge, there is no research paper about UCNPs with double efficient excitation bands for consecutive deep macroscopic and microscopic imaging.

Herein, we proposed specially-designed Er^{3+}-singly doped UCNPs which can achieve deep macroscopic imaging (excited at 808 nm CW) and microscopic imaging (excited at 1480 nm continuous wave (CW)) simultaneously by constructing a novel $NaYF_4:Er^{3+}@NaYF_4:Er^{3+}$ core–shell structure (as shown in Fig. 1(a)). The material structure and the excitation wavelength of Er^{3+}-singly doped UCNPs were further optimized to enhance the upconversion emission efficiency. To our experimental results, the efficiency of Er^{3+} is relative high (especially with high doping concentration of Er^{3+}) under excitation of which wavelength located around 808nm. This work demonstrated the feasibility of $NaYF_4:30\%Er^{3+}@NaYF_4:2\%Er^{3+}$ UCNPs as a class of promising optical probes in implementing simultaneous deep macroscopic and microscopic imaging.

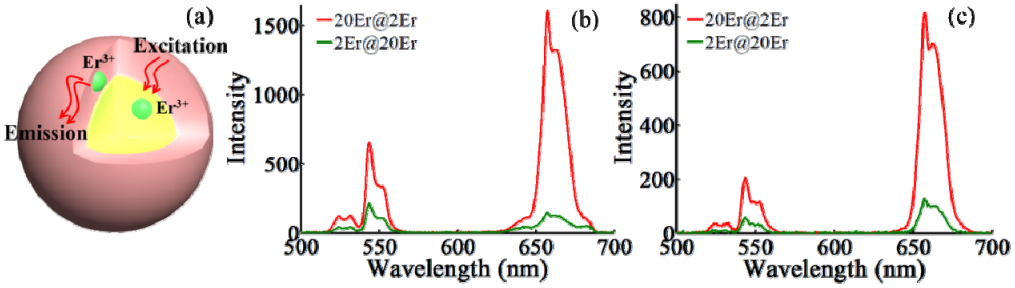

Fig. 1. (a) Schematic design of the simplex Er^{3+} -doped UCNPs architecture for simultaneous deep macroscopic and microscopic imaging. The upconverting emission spectra of $NaYF_4:20\%Er^{3+}$ $@NaYF_4:2\%Er^{3+}$ and $NaYF_4:2\%Er^{3+}@NaYF_4:20\%Er^{3+}$ UCNPs structures under (b) 808 nm CW (1.6 W) and (c) 1480 nm CW (248 mW) excitation, respectively.

2. Materials and method

2.1 Materials

Lanthanide chlorides ($YCl_3 \cdot 6H_2O$ and $ErCl_3 \cdot 6H_2O$ ≥99.9%) were purchased from Sigma-Aldrich. 1-octadecene (ODE) (≥90%), NH_4F was purchased from Aladdin Co, China. Oleic acid (AR), ethyl alcohol (AR), chloroform (AR), diethyl ether (AR), hydrochloric acid (AR) and acetone (AR) were purchased from Sinopharm Chemical Reagent Co., China. TiO_2 (AR) was purchased from Kermel, China. Regular agarose G-10 was purchased from BIOWEST, Spain. Deionized (DI) water was used in all the experimental procedures.

2.2 Synthesis of UCNPs

2.2.1 Synthesis of $NaYF_4:Er^{3+}@NaYF_4:Er^{3+}$

The $NaYF_4:Er^{3+}$ core was synthesized by a modified procedure obtained from the literature using oleic acid as coordinating ligands and 1-octadecene as noncoordinating solvent molecules [26]. Briefly, 1 mmol of $RECl_3 \cdot 6H_2O$ (RE = Y, Er) were mixed with 6mL of oleic acid and 15 mL of 1-octadecene in a 100 mL three-neck round-bottom flask. The dosages of $ErCl_3 \cdot 6H_2O$ and $YCl_3 \cdot 6H_2O$ depend on the doping concentration of Er^{3+} in the core. (In the case of the $NaYF_4:30\%Er^{3+}$ core, $YCl_3 \cdot 6H_2O$ (0.70 mmol) and $ErCl_3 \cdot 6H_2O$ (0.30 mmol) were applied). The mixture was then heated at 120 °C for 50 min before cooling to room temperature. Afterwards, 10 mL of methanol solution containing 4 mmol of NH_4F and 2.5 mmol of NaOH was added, and the solution was stirred at 50 °C for 30 min. Increase the temperature to 100 °C and keep the reaction mixture under vacuum (0.01 mbar) for 10 min to evaporate methanol. The solution was then heated to 315 °C for 90 min under the argon protection, then cooled rapidly, and 10 mL ethanol was added when the solution reached <75

#264009 Received 29 Apr 2016; revised 9 May 2016; accepted 9 May 2016; published 13 May 2016
(C) 2016 OSA

°C. Nanoparticles were precipitated by ethanol and collected by centrifugation at 7200 rpm for 4 min. Then the UCNPs were washed by ethanol several times and stored in 8 mL hexane (or chloroform).

The $NaYF_4:Er^{3+}$ shell was synthesized by a similar process, just adjusting the reaction temperature from 315°C to 290 °C. The dosages of $ErCl_3 \cdot 6H_2O$ and $YCl_3 \cdot 6H_2O$ depend on the doping concentration of Er^{3+} in the shell. (In the case of $NaYF_4:30\%Er^{3+}@NaYF_4:2\%Er^{3+}$, $YCl_3 \cdot 6H_2O$ (0.98 mmol) and $ErCl_3 \cdot 6H_2O$ (0.02 mmol) were applied.)

2.2.2 Synthesis of $NaYF_4:0.5\%Nd^{3+}$, $20\%Yb^{3+}$, $2\%Er^{3+}@NaYF_4$

The synthesis procedure of the $NaYF_4:0.5\%Nd^{3+}$, $20\%Yb^{3+}$, $2\%Er^{3+}$ core was almost the same as the $NaYF_4:Er^{3+}$ core except the doping lanthanide ions and their dosages. And the synthesis procedure of the $NaYF_4$ shell was almost the same as that used to synthesize the $NaYF_4:Er^{3+}$ shell, except that $YCl_3 \cdot 6H_2O$ (1 mmol), were added to a mixture of OA and ODE in three-neck round-bottom flask, instead of $YCl_3 \cdot 6H_2O$ (0.98 mmol) and $ErCl_3 \cdot 6H_2O$ (0.02 mmol).

2.3 Hydrophilic process of the UCNPs

Oleate-capped $NaYF_4:30\%Er^{3+}@NaYF_4:2\%Er^{3+}$ core-shell nanocrystals in hexane (or chloroform) were transferred into the aqueous phase through a modified ligand-free protocol [27, 28]. This ligand-free protocol might achieve stronger overall upconversion luminescence and higher R/G ratio than the oleate-capped ones. Typically, 1 mL of $NaYF_4:30\%Er^{3+}@NaYF_4:2\%Er^{3+}$ core-shell nanoparticles dispersed in hexane (or chloroform) were dried in a 10 mL vial under gentle air gas flow. Deionized water (5 mL) was then added into the vial and its pH value was adjusted to 2-4 using 0.1 M HCl. The mixture was sonicated for about 2 h while maintaining the pH value at 2-4 by adding 0.1 M HCl. The carboxylate groups of the oleate ligand were gradually protonated to yield oleic acid. After completion of this procedure, diethyl ether was added into the aqueous solution to remove the oleic acid by extraction. The process was repeated several times until the solution become totally transparent. The ligand-free $NaYF_4:30\%Er^{3+}@NaYF_4:2\%Er^{3+}$ core-shell nanoparticles in the water dispersible fraction were recuperated by centrifugation at 9000 rpm for 10 min after precipitation with acetone. The product was then redispersed in acetone, centrifuged, and finally dispersed in deionized water.

2.4 Phantom preparation

The tissue phantom consisted of 0.5% agarose (typical phantom matrix material), 0.7 grams per liter (g/L) of TiO_2 (scatterers) and 25×10^{-6} liters of ink (absorbers) per liter of tissue phantom. The adopted TiO_2 concentration depended on the data in related research [29], which suggests a reduced scattering coefficient of 0.34 mm^{-1}. The absorption coefficient of the phantom was controlled within a range between 0.006 to 0.009 mm^{-1} [30], similar to that of human epidermis and dermis tissues, indicating that this phantom mimics human skin tissues well [31].

2.5 Cell culture and treatment

HeLa cells were routinely cultured in Dulbecco's Modified Eagle Medium (DMEM; Gibco) supplemented with 10% fetal bovine serum (FBS; Gibco) and 100 IU/mL penicillin–streptomycin. Cell cultures were performed at 37 °C in a humidified atmosphere containing 5% CO_2. The cells were trypsinized and replanted at a density of 1×10^6 cells/mL onto a confocal petri dish (35 mm) upon reaching confluence, and grown at 37 °C under 5% humidified CO_2 for 48 hrs. For UCNPs labeling, the cells were rinsed gently with pre-warmed phosphate buffered saline (PBS) and incubated with 200 μL 25 mM ligand-free UCNPs added in a diameter of 6-cm cell-dish with 4 mL DMEM for 12 hours at 37°C. After that, the cells were gently rinsed twice with pre-warmed PBS to remove excessive UCNPs.

#264009 Received 29 Apr 2016; revised 9 May 2016; accepted 9 May 2016; published 13 May 2016
(C) 2016 OSA

2.6 Two-photon luminescence spectroscopy and deep macroscopic imaging

The two photon emission spectra of UCNPs were recorded by a fiber spectrograph (QE65000, Ocean Optics) in the microscope system. A consistent UCNPs concentration (about 0.125 mmol/mL) was used to measure the upconverting emission spectra. The CW laser beam was generated from a tunable Ti: Sapphire laser (Mira HP, Coherent).The pump-power dependence was measured with an optically thin sample on the coverslip through a microscope. The beam profile after the objective was estimated to be a circle with the radius of 2 μm.

In vitro phantom imaging and *in vivo* imaging experiments were carried out in a home-made optical system, as shown in Fig. 2. The nude mouse was anesthetized by injecting chloral hydrate (5% aqueous solution, 100 μL) and immobilized on the imaging stage. The bright images and fluorescence images were captured individually. The fluorescence images were taken with 500 ms exposure time. The excitation laser is CW 808 nm diode laser (CNI, China). And appropriate optical filter (Semrock LL01-808-12.5) was employed to optimize the excitation light. In addition, the laser was expanded by using lens combination. The excitation power density for the laser were tuned to 2 mW/mm^2. A 700 nm short pass filter (Andover 700FL-07-50) was used as emission filter or in vivo imaging under the 808-nm laser excitation. The fluorescence image was obtained with a charge coupled device (CCD).

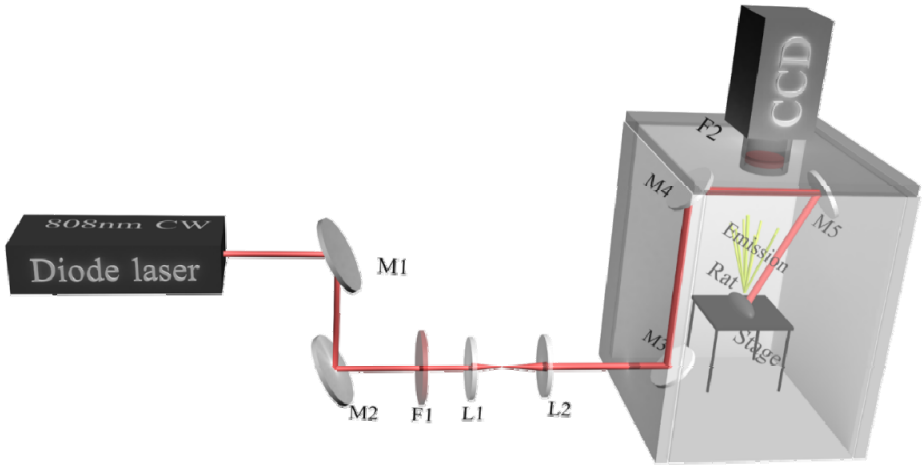

Fig. 2. The home-made optical system for deep macroscopic imaging (*in vitro* and *in vivo*). F1:808 nm band pass filter; F2: 700 nm short pass filter; L1: 25 mm focus lens; L2: 50 mm focus lens; M1, M2, M3: silver mirrors.

2.7 Three-photon luminescence spectroscopy and deep microscopic imaging

The three photon emission spectra of UCNPs were measured using a fiber spectrograph (QE65000, Ocean Optics) and excited with a 1480 nm CW diode laser (LEO Photonics, China). A consistent UCNPs concentration (about 0.125 mmol/mL) was used to measure the upconverting emission spectra. The pump-power dependence experiment was performed with an optically thin sample on the coverslip through a microscope. The beam profile after the objective was estimated to be a circle with the radius of 2 μm. This *in vitro* cell UC imaging experiment was implemented in the multiphoton laser scanning microscopy system (FV10MPE-S, Olympus) with 119.4 W/mm^2 output. Red and green UC photoluminescence from UCNPs were obtained using two channels with proper filters. The setup is illustrated in Fig. 9(a). The numerical aperture (NA) of the objective (20 × , 1.6 mm WD, Olympus) is 0.7.

#264009 Received 29 Apr 2016; revised 9 May 2016; accepted 9 May 2016; published 13 May 2016
(C) 2016 OSA

3. Results and discussions

3.1 Design and construction of the simplex Er^{3+} -doped UCNPs

According to the experimental results, the excitation efficiency of Er^{3+} is relatively high (especially for high Er^{3+}doping concentration) under CW excitation of which wavelength located around 808nm. Therefore, we firstly designed two kinds of Er^{3+} singly-doped core-shell structure UCNPs with high Er^{3+} doping concentration. One is heavily doped with Er^{3+} in the core ($NaYF_4$:20%Er^{3+}@$NaYF_4$:2%Er^{3+} (20Er@2Er for short)), while the other is doped with high-concentration Er^{3+} in the shell ($NaYF_4$:2%Er^{3+}@$NaYF_4$:20%Er^{3+} (2Er@20Er for short)). In order to figure out the better structure, the upconverting emission spectra of these two kinds of UCNPs were measured under 808 nm CW and 1480 nm CW excitations, respectively. As shown in Fig. 1(b) and 1(c), in both cases, the UCNPs gave intense green (543 nm, Er^{3+}: $^4S_{3/2}\rightarrow{}^4I_{15/2}$) and red (657 nm, Er^{3+}: $^4F_{9/2}\rightarrow{}^4I_{15/2}$) emissions. The spectra showed that the structure 20Er@2Er exhibited much higher emission intensities than that of 2Er@20Er under both 808 nm CW and 1480 nm CW laser excitations, indicating heavily doped with Er^{3+} in the core can achieve higher emission efficiency. Herein, Er^{3+} simultaneously served as activators and sensitizers, but played different roles in the core and the shell, respectively. Usually, activators need to be constrained in relatively low concentration (such as 1%, 2%), while sensitizers need for relatively high one (such as 18%, 20%). Therefore, the concentration would determine the role that Er^{3+} played in different layers. For 2Er@20Er, Er^{3+} acted as sensitizers in the shell layer where surface quenching effect occurred, leading to low efficiency. By comparison, Er^{3+}served as sensitizers in the core of 20Er@2Er. Without any surface defects in the core, the sensitizers went through much less quenching processes than that in 2Er@20Er and could be efficiently excited. That was the reason why 20Er@2Er exhibited higher emission efficiency, and we would adopt this kind of structure (heavily Er^{3+} -doped in core) for the following experiments.

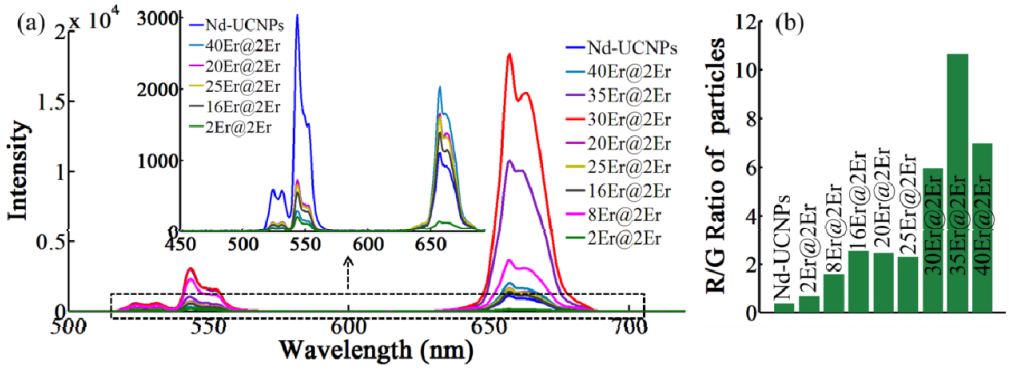

Fig. 3. The upconverting emission spectra (a) and the R/G ratio (c) of $NaYF_4$:x%Er^{3+}@$NaYF_4$:y%Er^{3+} and $NaYF_4$:0.5%Nd^{3+}, 20%Yb^{3+}, 2%Er^{3+}@$NaYF_4$ excited by 808 nm CW laser (1.6 W). (b) The enlarged image of the overlapped part in (a).

Afterwards, we synthesized a series of simplex Er^{3+} -doped UCNPs ($NaYF_4$:x%Er^{3+}@$NaYF_4$:2%Er^{3+} (xEr@2Er for short)) to optimize the structure by varying the Er^{3+} doping concentration inside the core with a fixed Er^{3+} concentration in the shell. Furthermore, $NaYF_4$:0.5%Nd^{3+}, 20%Yb^{3+}, 2%Er^{3+}@$NaYF_4$ (Nd-UCNPs for short), as a class of well-known efficient 800 nm-excited UCNPs [32], was synthesized to make a comparison with this series of simplex Er^{3+} -doped UCNPs. With the increase of doped Er^{3+} in the core, the upconverting emission of the synthesized simplex Er^{3+} -doped UCNPs generally became stronger and reached a peak in 30Er@2Er under 808 nm CW excitation, as shown in Fig. 3(a). Such emission gradually decreased as the Er^{3+} concentration rose to 40%. This indicated that the increase of doped Er^{3+} would quench the upconverting process, even when the total photon

#264009 Received 29 Apr 2016; revised 9 May 2016; accepted 9 May 2016; published 13 May 2016
(C) 2016 OSA

absorbance at 808 nm CW was raised. Significantly, we found that 30% Er^{3+} doped in the core was the optimal concentration and showed a 16.6-fold enhancement for the red emission and an equally strong green emission compared with the prepared Nd-UCNPs sample. Besides, the red/green (R/G) ratio of $NaYF_4$:x%Er^{3+}@$NaYF_4$:2%Er^{3+} was remarkably enhanced with the increasing Er^{3+} doping concentration in the core, indicating that simplex Er^{3+} -doped UCNPs would be a better choice for *in vivo* imaging, as shown in Fig. 3(b). It might achieve larger imaging depth than most of the green/blue-emission dominating UCNPs which would reduce the penetration depth caused by the strong reabsorption and rescattering of green/blue light in biological tissue [33].

A similar changing process involved in the upconverting emission intensity of the synthesized Er^{3+}-singly doped UCNPs when excited by 1480 nm CW laser (Fig. 4(a)). However, Nd-UCNPs did not show any emission under 1480 nm CW excitation, due to the lack of proper sensitizer. Taken together, these results explicitly implied that 30% Er^{3+} doped UCNPs was the optimal concentration when excited with the two lasers, 808 nm CW and 1480 nm CW. The size and morphology of 30Er@2Er were characterized by TEM, where the core UCNPs ($NaYF_4$:30%Er^{3+}) clearly exhibited a uniform, spherical shape with an average diameter of 27.1 nm (Fig. 4(b)). After being coated with a ~4 nm $NaYF_4$:2%Er^{3+} shell, the nanoparticles were approximately 34.3 nm in size and still present a uniform morphology (Fig. 4(c)).

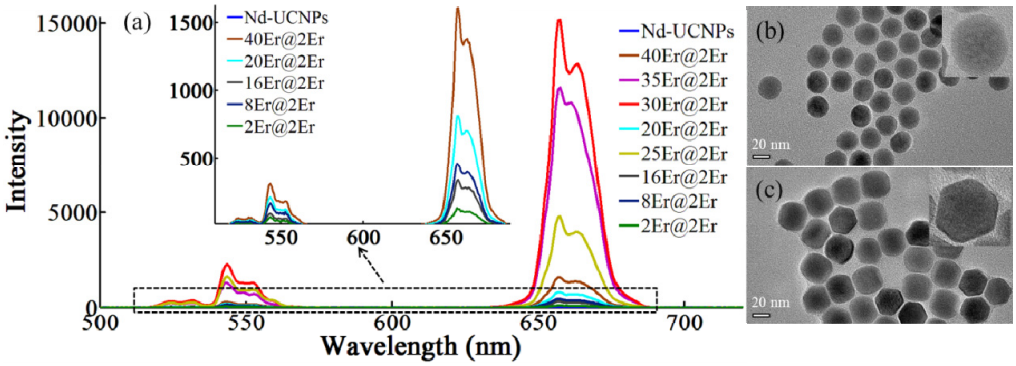

Fig. 4. (a) The upconverting emission spectra of $NaYF_4$:x%Er^{3+}@$NaYF_4$:2%Er^{3+} and Nd-UCNPs excited with 1480 nm CW (248 mW). The TEM image of (b) the core and (c) core-shell of the as-prepared $NaYF_4$:30%Er^{3+}@$NaYF_4$:2%Er^{3+} UCNPs.

For the sake of acquiring a highly efficient upconverting luminescence (UCL) for UCNPs, the excitation wavelength was also optimized, by the mean of measuring the upconverting emission spectra of 30Er@2Er UCNPs under different excitations (Fig. 5). As shown in Fig. 5 (inset), the red emission intensity variation revealed a crystal clear change trend upon altering excitation wavelength (from 790 to 814 nm CW). The maximal intensity was achieved when excited by 808 nm CW laser. And the UCL intensity rapidly declined at longer wavelength, which was ascribed to the mismatch between the excitation wavelength and the ground state absorption band of Er^{3+}.

#264009 Received 29 Apr 2016; revised 9 May 2016; accepted 9 May 2016; published 13 May 2016
(C) 2016 OSA

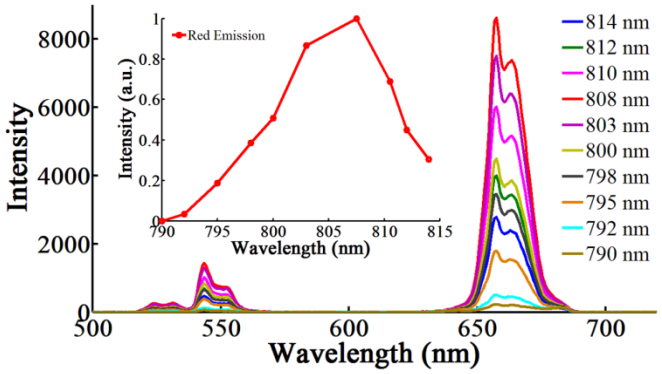

Fig. 5. The upconverting emission spectra and the red emission intensity change (inset) of $NaYF_4$:30%Er^{3+}@$NaYF_4$:2%Er^{3+} UCNPs under different wavelength excitation (1.6 W).

To investigate the upconversion mechanism of green and red emission for the 30Er@2Er UCNPs, the dependences of the emission intensities on pump power were measured. The relationship between luminescence intensity and excitation power can be described by the formula $I \propto P^n$, where I is the emission intensity, P is the pump power, and n is the number of photons involved in the excitation process [34]. The n was calculated by measuring the emission images in the microscope system and its corresponding pump laser power, and the results were used to draw a double-logarithmic plot in which the slope was n. Power dependence investigations of the 30Er@2Er UCNPs showed that both red and green emissions of Er^{3+} are governed by two-photon excitation upconversion processes under excitation with an 808 nm CW laser (the laser power densities range from 39.8 to 79.6 kW/mm^2) (Fig. 6(a)). The slopes are 1.96 for the detected red emission and 1.92 for the detected green emission, respectively. When excited with a 1480 nm CW laser (the laser power densities range from 13.9 to 83.6 W/mm^2), similar linear relations have been shown in Fig. 6(b). But slopes increased to 2.84 for the detected red emission and 2.71 for the detected green emission, respectively, which indicate three-photon processes for both red and green emission.

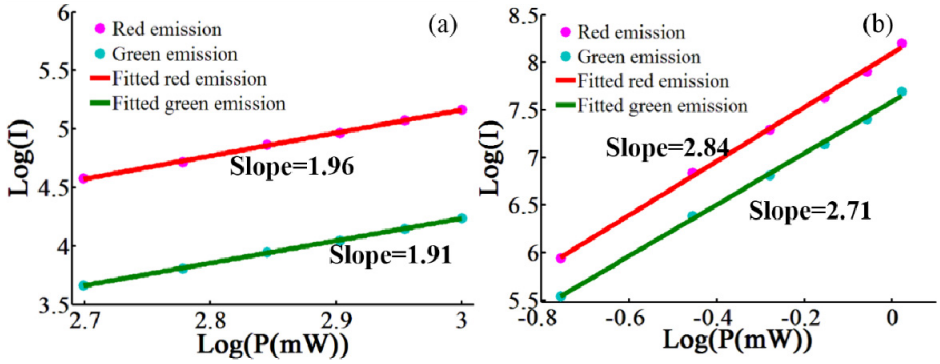

Fig. 6. Power dependence of $NaYF_4$:30%Er^{3+}@$NaYF_4$:2%Er^{3+} UCNPs under (a) 808 nm CW and (b) 1480 nm CW excitation, respectively.

#264009 Received 29 Apr 2016; revised 9 May 2016; accepted 9 May 2016; published 13 May 2016
(C) 2016 OSA

3.2 2PE deep macroscopic imaging

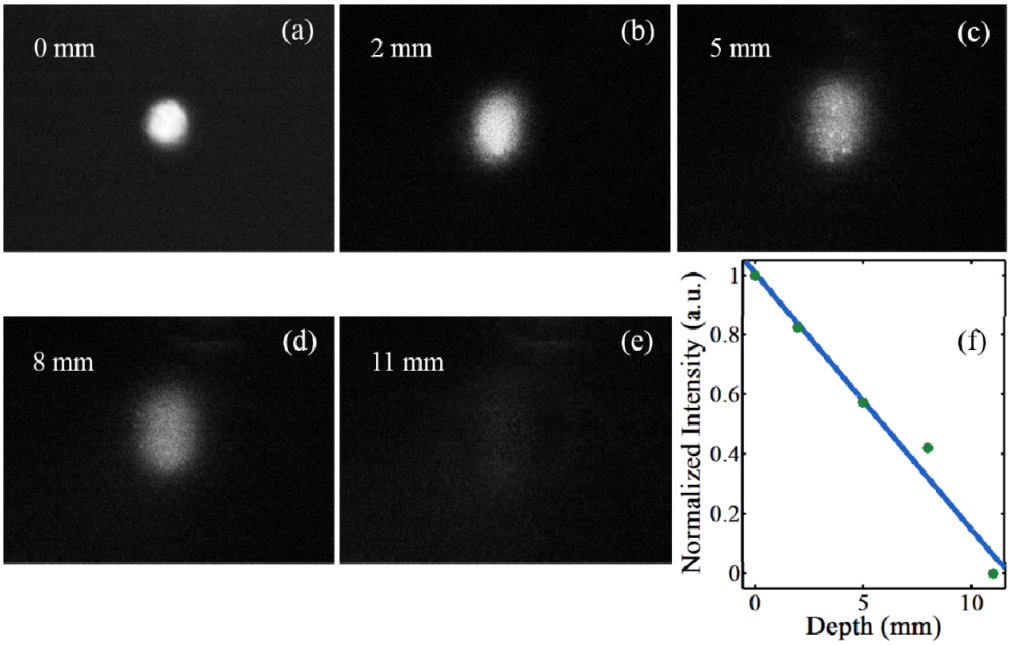

Fig. 7. Tissue penetration depth tests carried out in agarose phantom. The $NaYF_4$:30%Er^{3+}@$NaYF_4$:2%Er^{3+} NPs sample sealed in a capillary was inserted into the phantom at different depths, and the UC images (a-e) were then took by IVIS, under 808 nm laser irradiation (operated at power density of 2 mW/mm^2). (f) Attenuation of the measured fluorescence intensity with depth.

Compared to visible and ultraviolet light, NIR light that is within the optical transparency window (700-1100) has relatively low tissue absorption and thus high penetration depth, which is particularly desirable for biological detection and imaging [35, 36]. In the experiments, we used artificial phantom consisted of agarose (matrix) and TiO_2 (scatterers) to evaluate the imaging depth of 808 nm light excitation. A capillary filled with as-synthesized 30Er@2Er nanoparticles as photoluminescence inclusion was embedded in the phantom at five different depths (0, 2, 5, 8 and 11 mm). The well-prepared samples were imaged with a home-built optical system equipped with an 808 nm CW laser (2 mW/mm^2), as shown in Fig. 2. At each depth the UC photoluminescence image was acquired by CCD. With the increasing depth of UCNP inclusion, a monotonous decrease of the collected signal is observed. Finally the signal disappeared in the depth of 11 mm (Fig. 7). Because lights are attenuated within the phantom tissue, a deeper position requires that both the excitation and emission lights have to experience much more scattering and absorption. This observation promises 30Er@2Er NPs as an ideal class of bioprobes for *in vivo* imaging under 808 nm irradiation.

To demonstrate the capability of ligand-free 30Er@2Er NPs for *in vivo* bioimaging, we subcutaneously injected NPs dispersion into a nude mouse (20 mg/mL, 50 μL) at an injection depth of 3 mm (estimated by the syringe needle). Figure 8 presents the *in vivo* whole-body images of a nude mouse subcutaneously injected with the ligand-free 30Er@2Er NPs. A clear high-contrast PL picture was observed, and the bright emission arose from the place where 30Er@2Er NPs were injected (the luminescent trace of the injection needle could be distinguished). This implies that the great potential of 30Er@2Er NPs for deep macroscopic imaging including autofluorescence-free UC animal imaging.

#264009 Received 29 Apr 2016; revised 9 May 2016; accepted 9 May 2016; published 13 May 2016
(C) 2016 OSA

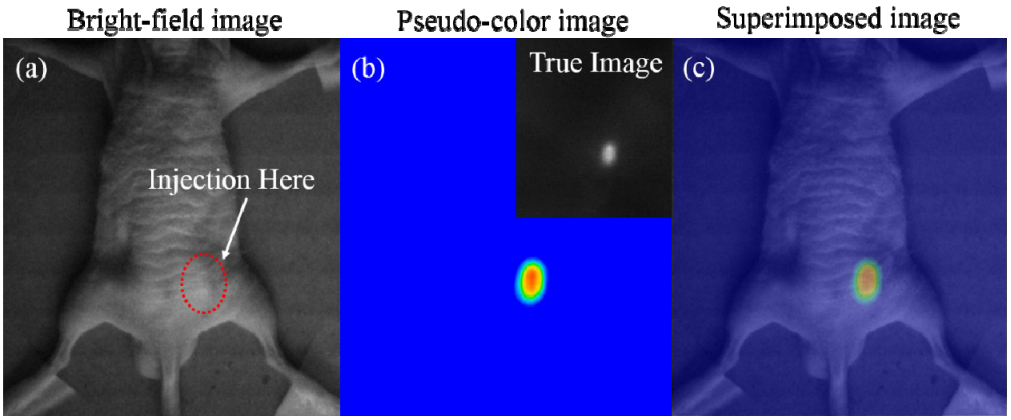

Fig. 8. *In vivo* whole-body images of a $NaYF_4$:30%Er^{3+}@$NaYF_4$:2%Er^{3+} injected nude mouse: (a) bright field image, (b) pseudo-color image obtained from true image (the inset black/white image), and (c) superimpose image (bright field image and pseudo-color image).

3.3 3PE deep microscopic imaging

To implement deep tissue microscopy, a layer of highly scattered agarose phantom was used. And two pieces of coverslip were utilized to shape the phantom as well as to conveniently control the phantom thickness. The cancer cells were cultured on a coverslip to minimize the refraction effect of the culture disk bottom, as shown in Fig. 9(a). A modified ligand-free protocol was adopted to make the 30Er@2Er UCNPs hydrophilic in this work. And the hydrophilic UCNPs were redispersed in deionized water. Then, the ligand-free UCNPs were cultured with HeLa cells for 12 hours before the microscopic imaging. The UCNPs-conjugated cancer cells imaging in *in vitro* microscopy were performed without phantom before deep microscopic imaging. Since the limitation of the detection wavelength range of photomultiplier tube (PMT), we could not obtain the transmission channel images under CW excitation at 1480 nm. However, it did not affect the detection of the luminescence signals as shown in Fig. 9(b). The signals of red and green emission via 3PE were strong and the images showed a relatively high contrast. The cells maintained in long-strip shape, a symbol of healthy cells, indicating that the ligand-free UCNPs were easily endocytosed by cells and hardly have cytotoxicity [28].

After that a 500-μm-thick phantom was applied, and the high contrast UCNPs-probed fluorescence imaging of cancer cells with a size of 512 × 512 pixels were obtained (Fig. 9(c)). The outlines of UCNPs-conjugated cells could also be observed clearly. This imaging depth was affected by several factors. Low NA, increased reflection and Fresnel refraction that resulted from the presence of several air-glass interfaces between the sample and the objective. Also a low power output (1.5 mW) of the objective would degrade the SNR of the images. After penetrating a layer of phantom, the excitation intensity would be much attenuated. As shown in Fig. 9(b), the intensity of green channel was equivalent to that of red channel when imaging directly on the cancer cells. By comparison, the green emission was much lower than the red one after penetrating the 500-μm phantom, as shown in Fig. 9(c). The red light has weaker attenuation than the green one in the biological tissue and is more suitable for deep bioimaging. All these results demonstrated that 30Er@2Er UCNPs could be applied to deep tissue microscopic imaging. Relatively high-contrast deep tissue microscopic images could be acquired by three-photon excitation with a 1480 nm CW laser.

#264009 Received 29 Apr 2016; revised 9 May 2016; accepted 9 May 2016; published 13 May 2016
(C) 2016 OSA

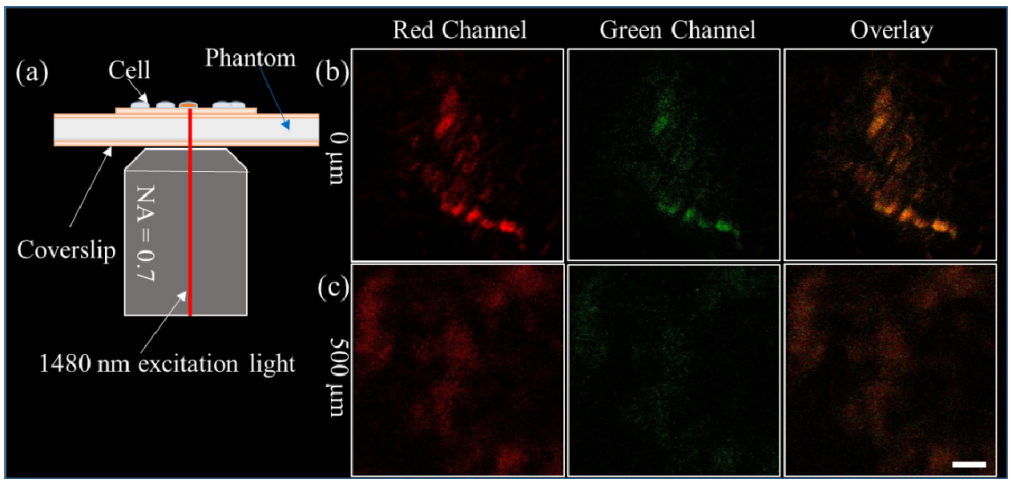

Fig. 9. (a) Schematic diagram for the setup of the objective, phantom and the cells on the coverslip. (b) *In vitro* cancer cell 3PM imaging without phantom. (c) *In vitro* cancer cell 3PM image based on a layer of 500 μm phantom (from left to right, red channel, green channel and overlay images, respectively.). The scale bar is 10 μm.

4. Conclusion

In conclusion, we have for the first time proposed specially-designed Er^{3+}-singly doped UCNPs which enables both deep macroscopic imaging (excited with an 808 nm CW laser) and deep microscopic imaging (excited with a 1480 nm CW laser) by the construction of a $NaYF_4:Er^{3+}@NaYF_4:Er^{3+}$ core–shell structure. The nanostructure, nanocomposites and the excitation wavelength of Er^{3+}-singly doped UCNPs have been systematically optimized to enhance the upconversion emission efficiency. According to the experimental results, the efficiency of Er^{3+} is relatively high (especially heavily doped with Er^{3+}) under excitation around 808 nm. To validate the feasibility of Er^{3+}-singly doped UCNPs applying as bioprobe, *in vitro* cell imaging and *in vivo* imaging have also been implemented. The present work has demonstrated the practicability of applying $NaYF_4:30\%Er^{3+}@NaYF_4:2\%Er^{3+}$ UCNPs as a class of promising optical probes in simultaneous macroscopic and microscopic imaging of deep tissue.

Acknowledgements

This work was supported by the National Natural Science Foundation of China (61405062, 61471186, 91233208), the Guangdong Innovative Research Team Program (201001D104799318), the Guangdong Natural Science Foundation of Guangdong province (S2013040014211, 2014A030313445), the China Postdoctoral Science Foundation (2013M530368, 2014T70818), and the Discipline and Specialty Construction Foundation of Colleges and Universities of Guangdong Province (2013LYM_0017).